Interface energy determination for the fully coherent β'' phase in Al–Mg–Si: making a case for a first principles based hybrid atomistic modelling scheme

F. J. H. Ehlers[1], S. Dumoulin[2], K. Marthinsen[3], and R. Holmestad[1*]

[1]Department of Physics, Norwegian University of Science and Technology (NTNU), 7491 Trondheim, Norway

[2]SINTEF, Materials and Chemistry, 7465 Trondheim, Norway

[3]Department of Materials Science and Engineering, Norwegian University of Science and Technology (NTNU), 7491 Trondheim, Norway

Abstract

We introduce a first principles based hierarchical multi-scale model scheme with application to a system comprising a fully coherent precipitate, immersed in a host lattice environment. As a test case, the needle-shaped main hardening phase β" in the Al–Mg–Si alloy system has been examined. Calculations were confined to a cross-section slab – where the coherency of the interfaces is well established experimentally. The scheme couples a density functional theory (DFT) based description of the interface vicinity to a linear elasticity theory (LET) based description of the larger surroundings as well as the precipitate interior. The establishing link between these descriptions is purely structural, and LET based. At the boundary between the DFT and LET regions, subsystem distortion energies were compared using both formalisms, revealing only weak differences. On the basis of the modelling results, the need of a multi-scale model scheme over a full DFT analysis has been quantified through analysis of the β" strain field decay. In the interface vicinity, and for a system comprising a β"–$Mg_5Al_2Si_4$ precipitate with 4 × 8 unit cells along $\mathbf{a}_P$, $\mathbf{c}_P$, respectively, the calculated interface energy of 2.36 kJ per mole exceeds predictions as obtained

with presently available alternative model schemes by ≈ 20%. Model system changes, required in order to approach a more reliable DFT-LET coupling and clarify the above described interface energy sensitivity, have been discussed. In comparison with alternative frameworks, our scheme offers additional flexibility when addressing interface configuration stabilities. This may allow for studying more realistic configurations in the future.

* Corresponding author. Email address: randi.holmestad@ntnu.no (R. Holmestad)

1. Introduction

Computational resources have advanced in recent years, to the point where first principles based theoretical studies of systems containing several hundred atoms are now routinely performed, and even larger systems starting to become tractable. Accordingly, modelling frameworks are increasingly focussing on the description of extended defects, and how to correctly model all important features of a physical system. In all aspects of fundamental alloy atomistic behaviours – whether studies of cracks, grain boundaries or precipitation – *hybrid model schemes* [1–3] are being proposed as efficient solutions to matching the dispersed long range strain effects self-consistently to the comparatively compact region of the defect itself. These schemes merge two basic features of the problem: far away from the defect, linear elasticity theory (LET) may suffice to describe the weak distortions of the host material away from its bulk state. By contrast, in the vicinity of the defect, *ab initio* methods are strictly needed to quantify the electronic effects of regions changed far away from this state. Crucially, these two regions should be linked through a seamless boundary condition in order to avoid introducing effects connected with mere model simplification [1].

For age hardenable alloy systems, precipitate-host lattice interface energies represent parameters of fundamental importance to integrated computational materials engineering [4–6]. In contrast to the

evident and challenging hybrid scheme problems where system dynamics, evolving defects and bond-breaking play key roles [7–9], [3], interface energy determination for a fully coherent precipitate-host lattice interface has up to now been treated in a decoupled manner. The presently most advanced model scheme [10] computes the (zero temperature) interfacial energy from density functional theory (DFT) based studies of local interface regions, while subsystem strain interactions relating to the full system are determined separately with LET. Despite the close subsystem structural similarity underlying the problem, the level of accuracy may still be importantly increased if a hybrid scheme were used for a *combined* determination of these quantities. Recent work by Ehlers and Holmestad [11] for the fully coherent needle shaped β" phase in the Al–Mg–Si alloy system stressed this possibility by highlighting (*i*) physically unacceptable boundary conditions in the DFT based studies and (*ii*) the importance of modelling the whole interface with DFT. A scheme for DFT calculations in a nm-thin shell – the *'interface region'* – enclosing the full precipitate-host lattice interface was provided. The authors however did not propose any scheme for establishing a communication between the interface region and the subsystem strain fields, needed to improve point *(i)*.

In the present paper, we introduce and evaluate the performance of a hierarchical multi-scale model scheme for the β"/Al system, building upon the work in [11]. Choosing computational simplicity over an attempted full hybrid scheme implementation, we select the structural information obtained from an LET modelling of the full system as the basis for the construction of the interface region supercells. Compared to [11], this modification provides a direct link to the surrounding strain field, albeit at the price of suppressing any influence of DFT related effects on the supercell dimensions. We stress that the precipitate induced strain field into the host lattice decays rapidly close to the interface but weakly at larger distances. Provided that electronic interface effects are essentially contained in the interface region, this indicates that DFT studies are needed only for this part of the

system. Making use of the presumed full coherency of precipitate and host lattice along the β" main growth (needle) direction, we limit modelling to a β"/Al cross-section region. Results are compared with those obtained from a study closely resembling [10].

The paper is managed as follows: in section 2, we introduce the β"/Al system and present the model strategies. In section 3, computational details are described, while calculated structures and energies for the β"/Al system are included in section 4. Here, also the comparison with alternative methods is performed. Section 5 provides comments on the precision of the scheme, as well as possible improvements towards a hybrid scheme set-up. Comparative advantages of presently available schemes from this category are considered. In section 6, we summarize the work. The paper includes three appendices. Appendix A and B present important simulation input and output data, respectively, while Appendix C discusses the influence of interface electronic effects on structural parameters.

2. Modelling strategies

2.1. The β'' precipitate

The fully coherent β" phase is the main hardening phase in the Al–Mg–Si alloy system [12, 13]. The orientation relationships between precipitate (P) and Al host lattice (H) were originally identified by Edwards *et al.* [14]:

$$[230]_{Al} \parallel [100]_{\beta''};\ [001]_{Al} \parallel [010]_{\beta''};\ [-310]_{Al} \parallel [001]_{\beta''}. \quad (1)$$

Subsequently, the monoclinic β" structure was determined [15, 16], revealing significant *misfits* between some of the precipitate unit cell and host lattice supercell lengths:

$$\mathbf{a}_P = (1+m_\mathbf{a})[2\mathbf{a}_{Al} + 3\mathbf{b}_{Al}] = (1+m_\mathbf{a})\mathbf{a}_H, \quad (2)$$

$$\mathbf{b}_P = (1+m_\mathbf{b})\mathbf{c}_{Al} = (1+m_\mathbf{b})\mathbf{b}_H, \quad (3)$$

$$\mathbf{c}_P = (1+m_\mathbf{c})[-(3/2)\mathbf{a}_{Al} + (1/2)\mathbf{b}_{Al}] = (1+m_\mathbf{c})\mathbf{c}_H. \quad (4)$$

Here, $\{\mathbf{a}_H, \mathbf{b}_H, \mathbf{c}_H\}$ is the set of basis vectors for the face-centred cubic (fcc) Al supercell, constructed from the conventional basis set $\{\mathbf{a}_{Al}, \mathbf{b}_{Al}, \mathbf{c}_{Al}\}$ with the aid of equation (1) to have all basis vector directions (but not the lengths) identical to the β" unit cell set $\{\mathbf{a}_P, \mathbf{b}_P, \mathbf{c}_P\}$. The misfits $m_\mathbf{a}$, $m_\mathbf{c}$ in equations (2) and (4) were reported in [16] to attain values of 3.8% and 5.3%, respectively, with $m_\mathbf{b}$ in equation (3) 'negligible'. By construction, $m_\mathbf{a} = (|\mathbf{a}_P| - |\mathbf{a}_H|)/|\mathbf{a}_H|$, with $|\mathbf{x}|$ denoting the Euclidean norm of vector $\mathbf{x}$. Given that the misfit **ab** and **cb** interfaces are coherent [17], β" growth is severely restricted along $\mathbf{a}_P$, $\mathbf{c}_P$, explaining the phase needle morphology. The relations between the sets of basis vectors for the fcc Al conventional unit cell, the Al supercell and the β" conventional unit cell are provided in figure 1. When equation (1) is strictly fulfilled, the monoclinic angle β_P between $\mathbf{a}_P$ and $\mathbf{c}_P$ is 105.3°, while the angle between $\mathbf{a}_{Al}$ and $\mathbf{a}_P$ is 56.3°.

The exact composition of the β" phase is still a matter of debate. Early studies [16] suggested an Mg_5Si_6 composition. More recent combined experimental and theoretical work [18] has emphasized the presence of Al in the structure, with an $Mg_5Al_2Si_4$ composition suggested as shown in figure 1. A mixture of these (and potentially, more) compositions in the physical precipitate is probable [18]. Additional theoretical studies [11] have suggested that equation (1) is considerably closer fulfilled by β"–$Mg_5Al_2Si_4$, compared to β"–Mg_5Si_6. The theoretical studies of section 4 assume an $Mg_5Al_2Si_4$ composition throughout, primarily for simplicity.

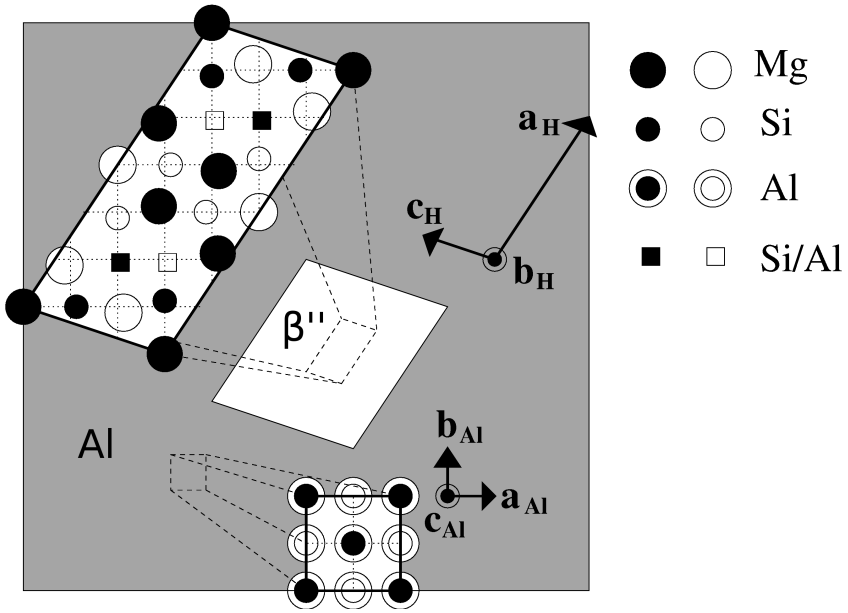

Figure 1. Basic structural details for the β"/Al system (β"/Al misfits neglected). The schematic presentation highlights the monoclinic β" conventional unit cell and the fcc Al conventional unit cell while also stressing the precipitate-host lattice orientation relationships through the connection between the fcc Al basis vectors {$\mathbf{a}_{Al}$, $\mathbf{b}_{Al}$, $\mathbf{c}_{Al}$} and the Al supercell basis vectors {$\mathbf{a}_H$, $\mathbf{b}_H$, $\mathbf{c}_H$} of equations (2) – (4). The cells are drawn on the same scale, with the basis vectors multiplied by a factor 1/2 by comparison. The β" basis vectors are obtained from the Al supercell basis vectors by the aid of equations (2) – (4). Two proposed β" compositions [16, 18] have been included: for β"–Mg_5Si_6 (β"–$Mg_5Al_2Si_4$) all squares in the precipitate unit cell denote Si (Al) atoms.

2.2. Full system geometry

For the LET modelling of the full β"/Al interaction induced strain field, we used the finite element method (FEM). The fully coherent β" precipitate has needle morphology (see section 2.1), with an experimentally reported [19] average length much larger (>10) than the average cross-section dimensions. Consequently, the displacement gradients, or strains, along the needle in both host lattice and precipitate generated during precipitation should be rendered much weaker, or even negligible relative to those generated in the cross-section plane. For simplicity, we model a 2D β"/Al cross-section slab only, assuming plane-strain (i.e. no strain along the third direction). The

slab has a thickness of one unit cell within each subsystem ($\mathbf{b}_P \approx \mathbf{b}_H \approx 0.405$ nm). Since the modelling assumes a homogeneous medium for each subsystem, optimization results are scale invariant, i.e., depending only on the *relative size* of these systems in the cross-section plane. Here, the host lattice region was chosen to be 11 × 11 times larger than the precipitate, in order to fully accommodate the strain field. To ease model construction, the geometrical shape of the host lattice was homothetic to the precipitate (see figure 2). Further, the precipitate-host lattice misfits were formally set to zero, i.e., $\mathbf{a}_P = \mathbf{a}_H$, $\mathbf{c}_P = \mathbf{c}_H$ in equations (2) and (4), respectively. Note that these relationships are only valid when the precipitate is homogeneously compressed and the host lattice not deformed.

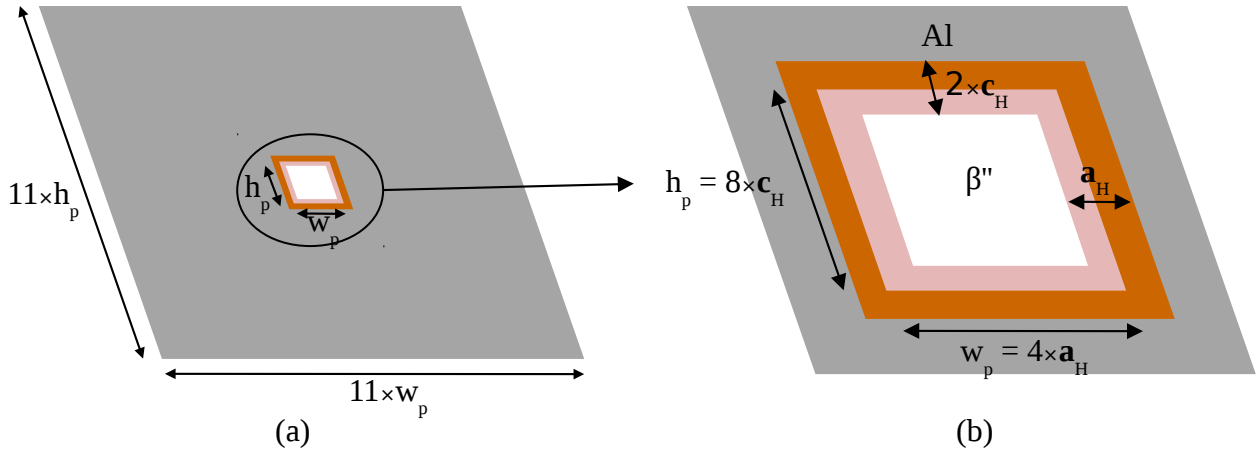

Figure 2. (*a*) Schematic presentation of modelling of the full system with (*b*) close-up on the precipitate. The precipitate has dimensions h_P, w_P. The highlighted areas extending into each subsystem from the precipitate-host lattice interface together represent the interface region.

In order to relate the chosen interface region extension (see section 3.2 for details) to the FEM based results, a choice is needed for the precipitate cross-section dimensions. In our simulations, we chose the size $4|\mathbf{a}_P| \times 8|\mathbf{c}_P|$, see figure 2(*b*). Using the experimental β" cell dimensions as a rough guideline [16], this amounts to ≈ 6 × 5.5 nm^2 – a precipitate above the reported average size [19]. At

the onset of structural optimization, the width of the interface region along the vertical (horizontal) interface in figure 2 is constant, attaining the value $\mathbf{a}_H$ ($2\mathbf{c}_H$), and shared evenly between the subsystems.

Relaxation of the system in figure 2 requires that the strains and stresses here be known. This starting point can be achieved following the Eshelby approach for inclusions [20]. Consider an infinite body with homogeneous properties (the 'matrix') of which a local region undergoes a transformation (e.g., precipitation), leading to a change of form and property (referred to as the 'inclusion') distinguishing it from the rest of the body. This transformation will change the previously stress-free configuration, i.e. stresses and strains will be generated inside and outside the inclusion. The solution to this problem is found via a sequence of imaginary cutting, straining and welding operations, as described in e.g. [20, 21]. This sequence is followed in the current study and is explained below. Numerous analytical solutions can be found in the literature but the case where both the materials are anisotropic with different elastic constants and the inclusion is of arbitrary shape is not treated due to its complexity.

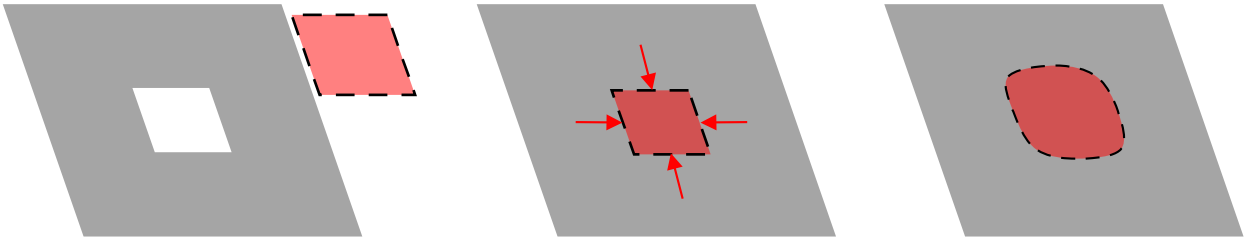

Figure 3. Schematic description of the (Eshelby) methodology followed in the modelling of the full system: (*a*) the precipitate is removed from the host lattice and let free to relax. (*b*) Displacements are applied at the precipitate boundary in order to fit into the host lattice. (*c*) The full system is relaxed.

In the present work, Eshelby's inclusion approach was solved as follows: firstly (figure 3(*a*)), the precipitate was removed from the host lattice and relaxed to its bulk structure. Secondly (figure 3(*b*)), an appropriate (compressive) displacement field was applied to the precipitate boundary in order to fit into the hole in the Al host lattice. The external surface of the precipitate and internal surface of the host lattice were then bonded together – i.e., the nodes belonging to each surface were merged – to ensure fully coherent interfaces. This procedure was straightforward as the subsystem meshes were built with this merging in mind. Finally (figure 3(*c*)), the full system was relaxed. For the determination of the stress-strain relations, LET was used throughout. Note that the first step is imaginary, with simulations performed only for the second and third steps. The calculations underlying this scheme require that the subsystem linear elastic constants be determined. In the present work, we used the elastic constants calculated in previous work by Ehlers and Holmestad [11], see table 3 in that paper for details.

2.3. The interface region

2.3.1. Probing the interface locally

The multi-scale model scheme of this work employs an FEM based description (see section 2.2) for the majority of the β"/Al system in figure 2, but the energies of the interface region shown in this figure are to be computed with *ab initio* methods. The use of LET for the remaining parts of the system attempts to ensure a smooth transition to the interface region: the bulk subsystem linear elastic constants underlying these LET simulations are *computed with DFT* [11], implying that in the limit of small distortions, the LET and DFT energy differences should be negligible.

For the case of a fully coherent precipitate possessing compositionally sharp and defect free planar interfaces with the surrounding host lattice, the modelling of an arbitrary *local* region on the interface was recently addressed by Ehlers and Holmestad [11]. The authors argued that an interface

region supercell focussing on the vicinity of a selected point on the interface under investigation can be determined for any given point away from the vicinity of the precipitate corners, by means of an appropriate distortion of this cell. The underlying cell construction generally employs the coupling of symmetrically equivalent local regions for the two interfaces of identical orientation (see figure 4(*a*)). By aid of interpolation at the precipitate corners, the scheme of [11] can hence describe the full interface, with *ab initio* theory and at an appropriate level of structural accuracy, provided that a reliable coupling to the strain field outside the interface region in figure 2 be made. For basic comments on the supercell construction, see section 3.2.

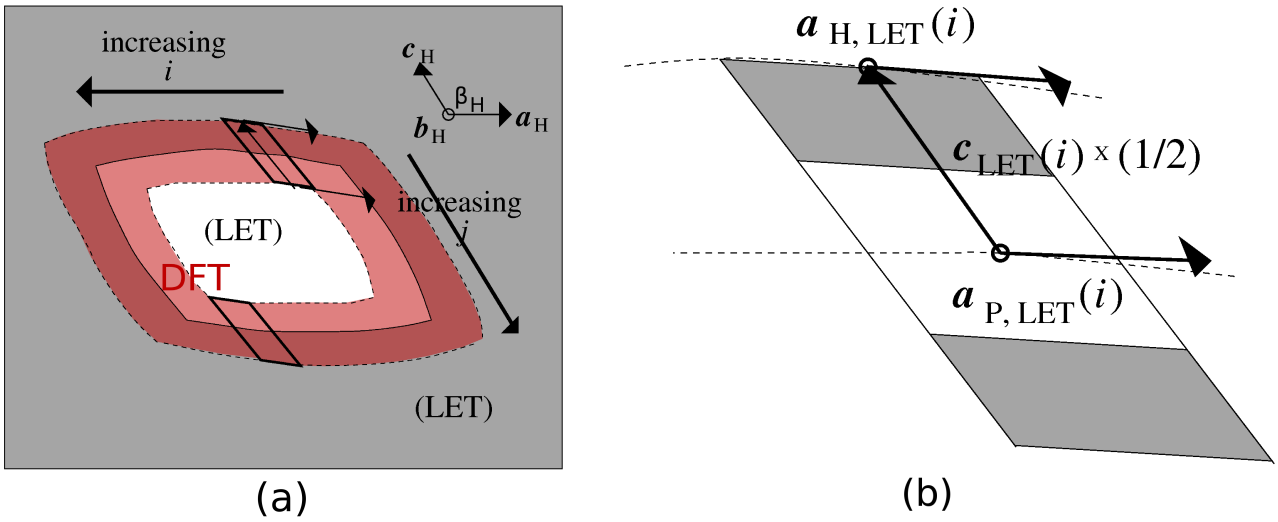

Figure 4. Schematic presentation of the structural boundary condition used for connecting interface region supercell distortions with a desired position on the interface, labelled with the real numbers *i* and *j* as shown. Following figure 2, precipitate and host lattice regions are emphasized with white and grey colour, respectively, while the interface region is delimited by dashed lines. (*a*) Fully relaxed β"/Al slab, as described with LET. The two symmetrically connected halves of the selected interface region supercell, shown in close-up in (*b*), have been highlighted with broad lines. The supercell is constructed [11] by adding together these halves and introducing periodic boundary conditions (PBCs) for the cell dimensions. Distortions have been exaggerated throughout.

The LET based calculations for the interacting β"/Al system differ fundamentally from the DFT based studies, with the latter (*i*) including structural distortions beyond the LET level as well as (*ii*) taking into account the electronic interactions of precipitate and host lattice. Even if one assumes that the electronic interface effects decay to negligible influence at the interface region boundaries in figure 4(*a*), a seamless coupling here still requires that a structural 'self-consistency loop' be implemented [22]. We choose a simplified approach to this problem below. Labelling the position on the **ab** and **cb** interfaces with the parameters *i* and *j*, respectively (see figure 4(*a*)), we determine both the cell basis vectors $\{\mathbf{a}^{\mathbf{ab}}(i), \mathbf{c}^{\mathbf{cb}}(j)\}$ (pointing along interface planes), as well as the vectors $\{\mathbf{c}^{\mathbf{ab}}(i), \mathbf{a}^{\mathbf{cb}}(j)\}$ (pointing out of interface planes) solely from LET. For details on the actual expressions, see section 2.3.3. The cell basis vectors $\mathbf{b}^{\mathbf{ab}}(i)$, $\mathbf{b}^{\mathbf{cb}}(j)$ (pointing out of the slab) – ambiguously defined in the calculations of section 2.2 when adopting the plane-strain approximation – are chosen as the average values of the two bulk subsystem counterparts:

$$\mathbf{b}^{\mathbf{ab}}(i) = \mathbf{b}^{\mathbf{cb}}(j) = (\mathbf{b}_{\mathrm{H}} + \mathbf{b}_{\mathrm{P}})/2. \tag{5}$$

The weights on $\mathbf{b}_{\mathrm{H}}$, $\mathbf{b}_{\mathrm{P}}$ in equation (5) reflect that all interface region supercells contain equal amounts of the two subsystems (see section 3.2).

Technically, the above described boundary condition assumes negligible structural effects of the subsystem electronic interactions, with such influences ignored entirely in the LET studies of section 2.2, and with no modification implemented in the DFT calculations. For discussions into the importance of this approximation, see Appendix C.

2.3.2. Interface region distortion parameters

For convenience in the context of analyses of the optimized precipitate-host lattice system, we introduce here three parameters describing the effects of the subsystem interactions on the set of interface region supercells, i.e., the local distortions in the vicinity of the interface. The presentation below aims at highlighting the (general) structural information contained in each parameter. In section 2.3.3, we will show how these quantities are obtained from the boundary condition of section 2.3.1.

For a cell describing the vicinity of point i on the **ab** interface, we define:

$$\mathbf{a}^{\mathbf{ab}}(i) = \mathbf{a}_{\mathrm{H}} + (1 - \psi^{\mathbf{ab}}(i))\times(\mathbf{a}_{\mathrm{P}} - \mathbf{a}_{\mathrm{H}}), \tag{6}$$

$$\mathbf{c}^{\mathbf{ab}}(i) = (4 + 2m_{\mathbf{c}})\mathbf{c}_{\mathrm{H}} + 2\kappa^{\mathbf{ab}}(i)\times(\mathbf{c}_{\mathrm{H}}/|\mathbf{c}_{\mathrm{H}}|) + 2im_{\mathbf{a},\mathrm{eff}}(i)\mathbf{a}_{\mathrm{H}}, \tag{7}$$

with corresponding equations for the supercell connected with point j on the **cb** interface:

$$\mathbf{a}^{\mathbf{cb}}(j) = (2 + m_{\mathbf{a}})\mathbf{a}_{\mathrm{H}} + 2\kappa^{\mathbf{cb}}(j)\times(\mathbf{a}_{\mathrm{H}}/|\mathbf{a}_{\mathrm{H}}|) + 2jm_{\mathbf{c},\mathrm{eff}}(j)\mathbf{c}_{\mathrm{H}}, \tag{8}$$

$$\mathbf{c}^{\mathbf{cb}}(j) = \mathbf{c}_{\mathrm{H}} + (1 - \psi^{\mathbf{cb}}(j))\times(\mathbf{c}_{\mathrm{P}} - \mathbf{c}_{\mathrm{H}}). \tag{9}$$

The precise meaning of the parameter i in equations (6) and (7), counted in units of movements of unit cells along the interface, is as follows: the value $i = 0$ implies the state of zero shear strain on the supercell, with an expected physical position close to the centre of the interface. By aid of the coherency relations, equations (2) and (4), this leads directly to $\mathbf{a}^{\mathbf{ab}}(0)$ ($\mathbf{c}^{\mathbf{ab}}(0)$) pointing along $\mathbf{a}_{\mathrm{H}}$ ($\mathbf{c}_{\mathrm{H}}$). The direction of increasing i has been outlined in figure 4(*a*). Normally, upon changing i, the directions of both cross-section plane basis vectors should be altered. However, since the supercell

can always be formally reoriented by a rotation around $\mathbf{b}_H$, we choose to let the interface plane basis vector $\mathbf{a}^{\mathbf{ab}}(i)$ in equation (6) point along $\mathbf{a}_H$ for all values of i for simplicity. For the case of $\mathbf{c}^{\mathbf{cb}}(j)$ and j in equations (8) and (9), equivalent considerations apply.

The parameters $\psi^{\mathbf{ab}}(i)$, $\psi^{\mathbf{cb}}(j)$ in equations (6) and (9), respectively, can now be seen as referring to the level of *precipitate adaptation* to the host lattice. For the extreme – and unrealistic – scenario $\psi^{\mathbf{ab}}(i) = \psi^{\mathbf{cb}}(j) = 1$ for all i, j, full adaptation is attained; $\mathbf{a}^{\mathbf{ab}}(i) = \mathbf{a}_H$; $\mathbf{c}^{\mathbf{cb}}(j) = \mathbf{c}_H$. While this information rigorously speaking applies to the interface region only, such a result would nevertheless strongly imply that the *full* β" precipitate adopted fcc Al cell dimensions. In other words, the effect of the subsystem interactions in figure 3(*c*) would be negligible, indicating an extremely soft precipitate. At the other extreme $\psi^{\mathbf{ab}}(i) = \psi^{\mathbf{cb}}(j) = 0$ for all i, j (no adaptation; $\mathbf{a}^{\mathbf{ab}}(i) = \mathbf{a}_P$; $\mathbf{c}^{\mathbf{cb}}(j) = \mathbf{c}_P$), an expansion of β" in figure 3(*c*) back to the original bulk state of figure 3(*a*) would be implied, i.e., an extremely hard precipitate. Given the similar β" and fcc Al elastic constants [11], one may, roughly speaking, expect $\psi^{\mathbf{ab}}(i) \approx \psi^{\mathbf{cb}}(j) \approx 0.5$.

The parameter $m_{\mathbf{a},\mathrm{eff}}(i)$ in equation (7) represents the *effective misfit* locally present between the interacting β" and fcc Al subsystems at point i on the **ab** interface. The associated term $2im_{\mathbf{a},\mathrm{eff}}(i)\mathbf{a}_H$ in equation (7), roughly describing the level of shear strain on the supercell, is a direct generalization of the proposed supercell distortion in [11]. The modification in the present work is the replacement of the bulk subsystem misfit $m_{\mathbf{a}}$ with $m_{\mathbf{a},\mathrm{eff}}(i)$, reflecting the changed boundary condition. Since the strain fields outside the interface region in figure 4(*a*) drive the subsystems toward (though not reaching) mutual adaptation, the equation $m_{\mathbf{a},\mathrm{eff}}(i) < m_{\mathbf{a}}$ should generally apply. Likewise, in equation (8), $m_{\mathbf{c},\mathrm{eff}}(j) < m_{\mathbf{c}}$.

Finally, the interface region *compression parameter* $\kappa^{\mathbf{ab}}(i)$ in equation (7) describes yet another level

of β" adaptation to the surrounding host lattice environment – namely, the extent to which the interface region is compressed normal (roughly) to the interface plane, relative to the individual bulk subsystem parts. For the case $\mathbf{c}^{\mathbf{ab}}(0)$, where the term $2\kappa^{\mathbf{ab}}(0)\times(\mathbf{c}_H/|\mathbf{c}_H|)$ is normal to the interface plane by construction, a zero value of $\kappa^{\mathbf{ab}}(0)$ will imply an interface region width of $(4 + 2m_c)|\mathbf{c}_H|$ – the contribution from the first term in equation (7). Returning to figure 2, this length corresponds to the result obtained if both subsystems assume their bulk state (in the figure, the β" compression reduces m_c to zero). Note that the supercell contains two interfaces, explaining the number 2 in front of $\kappa^{\mathbf{ab}}(i)$. The parameter $\kappa^{\mathbf{cb}}(j)$ in equation (8) is defined in the same manner. Generally, we would expect $\kappa^{\mathbf{ab}}(i), \kappa^{\mathbf{cb}}(j) < 0$ (hence the name 'compression parameter'), given that the precipitate is likely compressed along both cross-section basis vector directions.

2.3.3. Interface region structural boundary condition

For the interface region structural boundary condition introduced in section 2.3.1 to be properly established, a set of equations specifically relating the FEM output data to the interface region supercell dimensions in the cross-section plane is needed. Following the remarks in section 2.3.1, the cell dimension $\mathbf{a}^{\mathbf{ab}}(i)$ is defined by balancing the structural information from the two interface region boundaries present:

$$\mathbf{a}^{\mathbf{ab}}(i) = |(\mathbf{a}_{H,\,LET}(i) + \mathbf{a}_{P,\,LET}(i))/2|\times(\mathbf{a}_H/|\mathbf{a}_H|). \tag{10}$$

The subscript 'LET' in equation (10) stresses the connection to the FEM based calculation, with $\mathbf{a}_{H,\,LET}(i)$ ($\mathbf{a}_{P,\,LET}(i)$) being the tangent to the boundary between the interface region and the host lattice (precipitate) at point *i*, see figure 4(*b*). The averaging of these terms is required for the periodic boundary conditions (PBCs) underlying the supercell description to be enforced. Correspondingly, $\mathbf{c}^{\mathbf{cb}}(j)$ as obtained in this work, is given by:

$$\mathbf{c}^{\mathbf{cb}}(j) = |(\mathbf{c}_{\mathrm{H,\,LET}}(j) + \mathbf{c}_{\mathrm{P,\,LET}}(j))/2|\times(\mathbf{c}_{\mathrm{H}}/|\mathbf{c}_{\mathrm{H}}|). \quad (11)$$

Formally (section 2.3.1), $\mathbf{c}^{\mathbf{ab}}(i)$ is obtained directly from the FEM based optimization output. However, to highlight the details of the practical identification, we make use of the properties of figure 3(*b*). Here, the precipitate is compressed to fully match the host lattice and $\mathbf{c}^{\mathbf{ab}}(i)$ attains the same value, $\mathbf{c}_{\mathrm{H}}$, for all *i*. Firstly, we identify pairs of nodes in the FEM input data, located a distance $2\mathbf{c}_{\mathrm{H}}$ apart in the interface region (i.e., on adjacent boundaries to the precipitate and host lattice), and with the connecting line running through point *i* on the **ab** interface. Upon system relaxation, the vector connecting these same nodes equals $(1/2)\times\mathbf{c}^{\mathbf{ab}}(i)$. Similar considerations apply to the case of $\mathbf{a}^{\mathbf{cb}}(j)$.

The interface region distortion parameters introduced in section 2.3.2 can now be written in terms of output parameters from the FEM modelling. For the precipitate adaptation parameter $\psi^{\mathbf{ab}}(i)$, inserting equation (10) in equation (6) and using equation (2), we obtain:

$$\psi^{\mathbf{ab}}(i) = 1 - (1/m_{\mathbf{a}})(|(\mathbf{a}_{\mathrm{H,\,LET}}(i) + \mathbf{a}_{\mathrm{P,\,LET}}(i))/2|/|\mathbf{a}_{\mathrm{H}}| - 1). \quad (12)$$

To see how the effective misfit $m_{\mathbf{a},\mathrm{eff}}(i)$ and the compression parameter $\kappa^{\mathbf{ab}}(i)$ are obtained from $\mathbf{c}^{\mathbf{ab}}(i)$, we divide this vector onto components along $\mathbf{c}_{\mathrm{H}}$ and $\mathbf{a}_{\mathrm{H}}$:

$$\mathbf{c}^{\mathbf{ab}}(i) = \overline{P}_{\mathbf{c}}(\mathbf{c}^{\mathbf{ab}}(i))\times(\mathbf{c}_{\mathrm{H}}/|\mathbf{c}_{\mathrm{H}}|) + \overline{P}_{\mathbf{a}}(\mathbf{c}^{\mathbf{ab}}(i))\times(\mathbf{a}_{\mathrm{H}}/|\mathbf{a}_{\mathrm{H}}|). \quad (13)$$

Here, e.g. $\overline{P}_{\mathbf{a}}(\mathbf{x})$ denotes the operator projecting $\mathbf{x}$ onto $\mathbf{a}_{\mathrm{H}}$. Comparison of equation (13) with equation (7) now yields:

$$2im_{\mathbf{a},\mathrm{eff}}(i) = \overline{P}_{\mathbf{a}}(\mathbf{c}^{\mathbf{ab}}(i))/|\mathbf{a}_{\mathrm{H}}|, \tag{14}$$

$$\kappa^{\mathbf{ab}}(i) = (\overline{P}_{\mathbf{c}}(\mathbf{c}^{\mathbf{ab}}(i)) - (4 + 2m_{\mathbf{c}})|\mathbf{c}_{\mathrm{H}}|)/2. \tag{15}$$

The equations (12), (14) and (15) are readily generalized to the **cb** interface consideration, by permutation of all **c**'s and **a**'s (and *i*'s and *j*'s) involved and appropriate scaling of the last term for the $\kappa^{\mathbf{cb}}(j)$ equation.

2.4. Testing the quality of the DFT-LET coupling

The model scheme of figure 4(*a*) assumes that LET will be valid everywhere outside the interface region. Evidently, the point where this assumption is put to the greatest test will be at the boundary to this region – the shortest distance to the place where the two subsystems physically meet, and hence the location where the strain outside the interface region reaches the highest level. Along the two boundary lines present (one for each subsystem, see figure 5), we determine the level of subsystem distortions as predicted by the FEM modelling, subsequently comparing the resulting LET and DFT energy changes. If these differences are everywhere within an acceptable tolerance, the assumption of a smooth transition from DFT to LET based modelling is regarded justifiable. We stress that this 'DFT-LET boundary condition', while focussing on the distorted system energies, still implicitly assumes that interface electronic effects are negligible at the region boundaries.

Specifically, for the case of the **cb** interface region boundary to the host lattice (see figure 5), we derive the subsystem distortion to be used for the LET calculations (see, e.g. [23]) as:

$$e_1\ (= e_{\mathrm{xx}}) = |\mathbf{a}_{\mathrm{H,\ LET}}(j)|/|\mathbf{a}_{\mathrm{H}}| - 1, \tag{16}$$

$$e_3\ (= e_{zz}) = [|\mathbf{c}_{H,\,LET}(j)|\sin(\beta_{H,\,LET}(j))]/[|\mathbf{c}_H|\sin(\beta_H)] - 1, \quad (17)$$

$$e_5\ (= e_{zx}) = \{|\mathbf{c}_H|\cos(\beta_H) - |\mathbf{c}_{H,\,LET}(j)|\cos(\beta_{H,\,LET}(j))\}/\{|\mathbf{c}_H|\sin(\beta_H)\}. \quad (18)$$

Here, the label *j* denotes the movement along the boundary, similar to the label *j* used for the **cb** interface region calculations (though the paths traversed in the two cases are of different length). For the case of the boundary to β", equations (16) – (18) apply as well – for the set of optimized lengths and angles $\{|\mathbf{a}_{P,\,LET}(j)|, |\mathbf{c}_{P,\,LET}(j)|, \beta_{P,\,LET}(j)\}$ and modified initial structural parameters $|\mathbf{a}_P|$, $|\mathbf{c}_P|$ and β_P. Extension to the **ab** interface is straightforward.

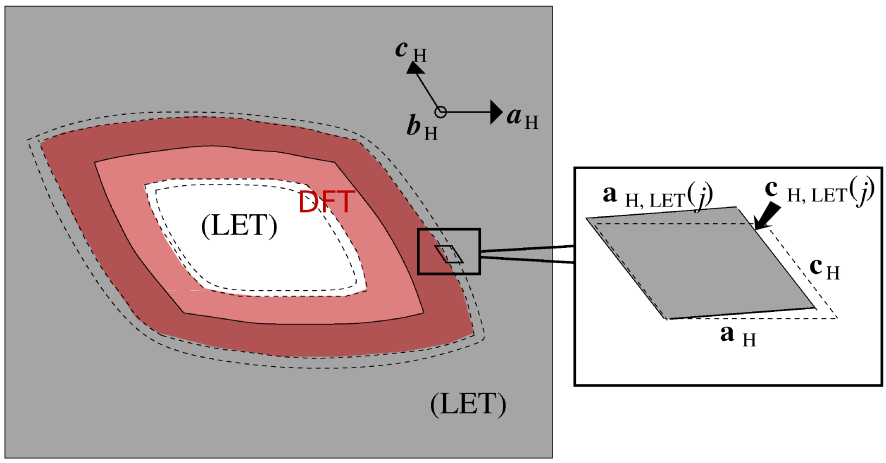

Figure 5. Schematic presentation of the determination of the level of host lattice strain at the interface region boundary. The basis vectors $\mathbf{a}_{H,\,LET}(j)$, $\mathbf{c}_{H,\,LET}(j)$ are computed from the studies described in section 2.2. Note that, generally, not only the lengths, but also the angle $\beta_{H,\,LET}(j)$ between these vectors has been altered compared to the bulk phase vectors $\mathbf{a}_H$, $\mathbf{c}_H$ (angle β_H).

3. Computational details

3.1. FEM based studies

For the FEM calculations, the finite element commercial code LS-DYNA [24] was used. We modelled the Al host lattice and β" precipitate using 30720 and 256 four-node plane-strain elements, respectively. The response of the subsystems to the misfit induced strain interactions was described using orthotropic elasticity. For each subsystem, the material directions were defined according to equations (2) and (4), with $\mathbf{a}_P$ being horizontal (see figure 2). All elastic constants were obtained from DFT based studies, see section 2.2. Note that the elastic response of an orthotropic material requires only 9 independent material parameters, i.e. c_{11}, c_{22}, c_{33}, c_{12}, c_{13}, c_{23}, c_{44}, c_{55} and c_{66} (as opposed to the 13 elastic constants for monoclinic β"). In addition, since plane-strain is assumed, the constants c_{44} and c_{66} do not play any role here, and hence were ignored.

Two potential sources of errors in the modelling were tested directly: to ensure that the strain field was fully accommodated, simulations were performed where the periphery of the system was either free to move or fully constrained; the difference in strain values thus obtained was in average $2 - 5 \times 10^{-4}$ while strains in the host lattice and the precipitate are of the order of a few percent (see section 4.1). At the precipitate-host lattice interface, the distances between the nodes located on the external surface of the precipitate and their counterparts on the internal surface of the host lattice (see section 2.2) were examined. The largest such distance was found to be less than 3×10^{-6} nm – almost certainly sufficiently small to be rendered negligible.

For the energy considerations of section 4.5, a cut-off for the strain field r_C is needed (in order to keep the strain energy contribution from diverging). This parameter was specified as the average distance from the precipitate centre where the effective strain – a quantity proportional to the norm of the strain tensor [24] – is 10 times lower than its maximum value. The use of relative values here ensures little influence on the particular quantity employed for the estimate. The procedure yields $r_C \approx 9.2$ nm, a value roughly 3 times the shortest distances from the precipitate centre to the interface.

For further discussions of this estimation, see section 4.5.

3.2. Choice of interface region supercell

The DFT based calculations of this work employ a sequence of interface region supercells for optimal description of all local regions on the interface, as described in section 2.3.1. Following the schematic presentation of the β" unit cell in figure 1 and the remarks on the chosen interface region width in section 2.2, it emerges that the **cb** interface cells should host one β" cell and one Al supercell of section 2.1, coupled along $\mathbf{a}_H$. At the point where β" is compressed to fully match the host (figure 2), this cell would have a dimension of $2|\mathbf{a}_H|$ along $\mathbf{a}_H$, i.e., two interface region widths. This is the desired value when comparing with section 2.2, as the supercell will incorporate two interfaces (figure 4). This cell contains 44 atoms. While the choice of interface region width is resting on earlier theoretical studies by Wang *et al.* [25], no independent cell size convergence studies have been carried out in our work. The main justification for the interface region extension is connected to the magnitude of the strain field components outside this region, see sections 4.1 and 4.2.

Following the same strategy as outlined above, an **ab** interface cell hosting two β" cells and two Al supercells can be constructed. Here, it is favourable to choose the β" primitive unit cell and the associated Al supercell as fundamental units, however: it follows directly from figure 1 that a smaller unit cell exists with

$$\mathbf{a}_P^{\text{Prim.}} = (1+m_{\mathbf{a}})(\mathbf{a}_{Al} + (3/2)\mathbf{b}_{Al}) + (1/2)\mathbf{c}_{Al} = (1/2)\mathbf{a}_P + (1/2)\mathbf{c}_{Al}. \quad (19)$$

The **ab** interface region supercell constructed from this smaller cell will contain 44 atoms only (as opposed to 88 if the β" conventional cell were used). In practice, both the **cb** and **ab** interface region

supercells were constructed from β" primitive supercells and the associated Al supercell, in order to keep the chosen method framework as similar as possible throughout. For the practical studies, identical interface configurations compatible with a stoichiometric precipitate were chosen for interfaces of the same orientation.

3.3. DFT based studies

For the DFT based [26, 27] calculations, the plane-wave (PW) based Vienna *Ab initio* Simulation Package (VASP) [28, 29], employing Vanderbilt ultrasoft pseudopotentials [30] and the Perdew-Wang generalized gradient approximation (GGA) [31] to the exchange-correlation functional was used. In all simulations, atomic positions in the cell were optimized. For the β" primitive unit cell, a 225 eV PW cut-off and a (12, 22, 14) Monkhorst-Pack *k*-point grid was chosen, with compatible *k*-point grids used whenever possible for the β"/Al interface region supercells. While the various cells along the interface are distorted differently, we stress that supercell volumes and monoclinic angles differ in total by only 0.3% and 3.3°, respectively (see Appendix B). This indicates little influence of finite sized PW basis set errors – a conclusion directly supported by calculations employing a 250 eV PW cut-off and 'High' precision setting, where the relative energy changes for the selected 'extreme' cells were found to be lower than 1 meV/cell. The *k*-point grid accuracy was tested in earlier work [11]. The optimized Al and β" structural parameters have been included in table A1.

4. Results and discussion

4.1. FEM relaxation results

The β" strain field as calculated with FEM is shown in figure 6. Using an orthonormal basis ($\mathbf{a}_P/|\mathbf{a}_P|$, $\mathbf{n}^{ab}{}_P$) with $\mathbf{n}^{ab}{}_P \bullet \mathbf{a}_P = \mathbf{n}^{ab}{}_P \bullet \mathbf{b}_P = 0$, both the unidirectional (figures 6(*a*) and (*b*)) and shear strain fields (figure 6(*c*)) are displayed. Given the positive β"/Al misfit values (see section 2.1), the

host lattice should be stretched along the interface and compressed in the normal direction. Correspondingly, the strain field along $\mathbf{a}_P/|\mathbf{a}_P|$ ($\mathbf{n}^{ab}{}_P$) shows tension (compression) of Al near the **ab** interface but compression (tension) near the **cb** interface. In figure 6(*c*), high shear strains of ≈ 5% are obtained at the precipitate corners. This might overestimate the strain in the physical system, as these corners were modelled as sharp with FEM. Figure 6(*d*) shows the strain field along $\mathbf{c}_P/|\mathbf{c}_P|$.

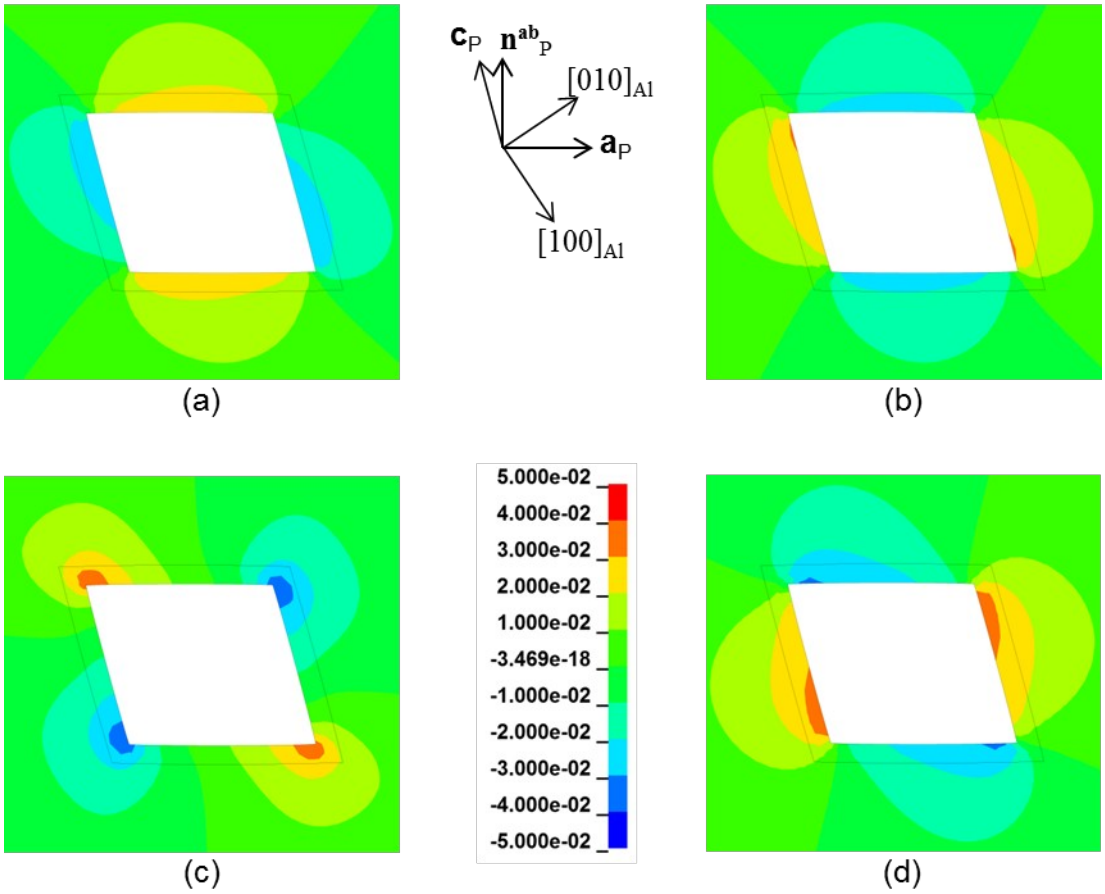

Figure 6. Strain field components in the fcc Al host lattice around the β" precipitate. Strain field along (*a*) the unit vector $\mathbf{a}_P/|\mathbf{a}_P|$ (i.e. direction $[230]_{Al}$) and (*b*) $\mathbf{n}^{ab}{}_P$ (direction $[-320]_{Al}$). (*c*) Shear strain in the basis $\{\mathbf{a}_P/|\mathbf{a}_P|, \mathbf{n}^{ab}{}_P\}$. (*d*) Strain field along $\mathbf{c}_P/|\mathbf{c}_P|$ (direction $[-310]_{Al}$). In all figures, the boundary between the interface region and the host lattice has been indicated with a thin line, with the precipitate covered by the white box shown.

It is of interest here to examine the β" induced strain field decay, in order to judge the necessity of a multi-scale model scheme for this system. Evidently, 'appreciable' strain field components, numerically exceeding 1%, are practically confined to the interface region, in support of DFT studies being needed only for this part of the system. At the same time, components numerically reaching 1% are still found at distances of ≈ 3 nm from the interface in figure 7 (beyond four times the distance of ≈ 0.7 nm from the interface to the interface region boundary). The effects of such levels of strain should be well described with LET, but the contribution to the full strain energy is likely non-negligible, indicating the need for a large model system. We shall quantify this latter consideration in section 4.5.

4.2. DFT-LET boundary condition

Following the procedure outlined in section 2.4, we obtained from the FEM studies of section 4.1 the structural distortions of the bulk Al and β" systems at the respective boundaries to the interface region (see figure 5). These distortions are shown in figures 7(*a*) and (*b*) (Al, β", respectively), with the contributions connected with e_1, e_3 and e_5 (see equations (16) – (18)) included separately to highlight the effects of compression vs. shear. The corresponding (LET and DFT) energy penalties relative to the fully optimized bulk subsystems have been included in figures 7(*c*) and (*d*). Note that, by choice, no cells are centred on the boundary edges in the analysis: for the β" boundary, this reflects that any overlapping with the interface region is avoided.

Keeping in mind that a permutation of e_1 and e_3 should be performed when focusing on a horizontal rather than a vertical boundary, the calculated variation of the distortions is highly similar for the individual subsystems. In the case of β" (figure 7(*b*)), a practically homogeneous compressive strain is observed across the entire boundary, with only the shear strain displaying significant variation. For the case of Al (figure 7(*a*)), a similar tendency is encountered, but only away from the

precipitate corners, where by contrast, a clear relaxation back towards the bulk subsystem is found. The curves in general are not fully symmetric around the centre position on the boundary, though a high level of symmetry still appears to be present for the Al (β") data if this point is shifted to a slightly higher (lower) value. As already discussed in section 4.1, the host lattice is stretched along the interface but compressed in the direction out of the interface, whereas the precipitate is compressed along both directions. The distortion energies are generally higher at the boundary to the precipitate, reflecting this lower degree of structural relaxation.

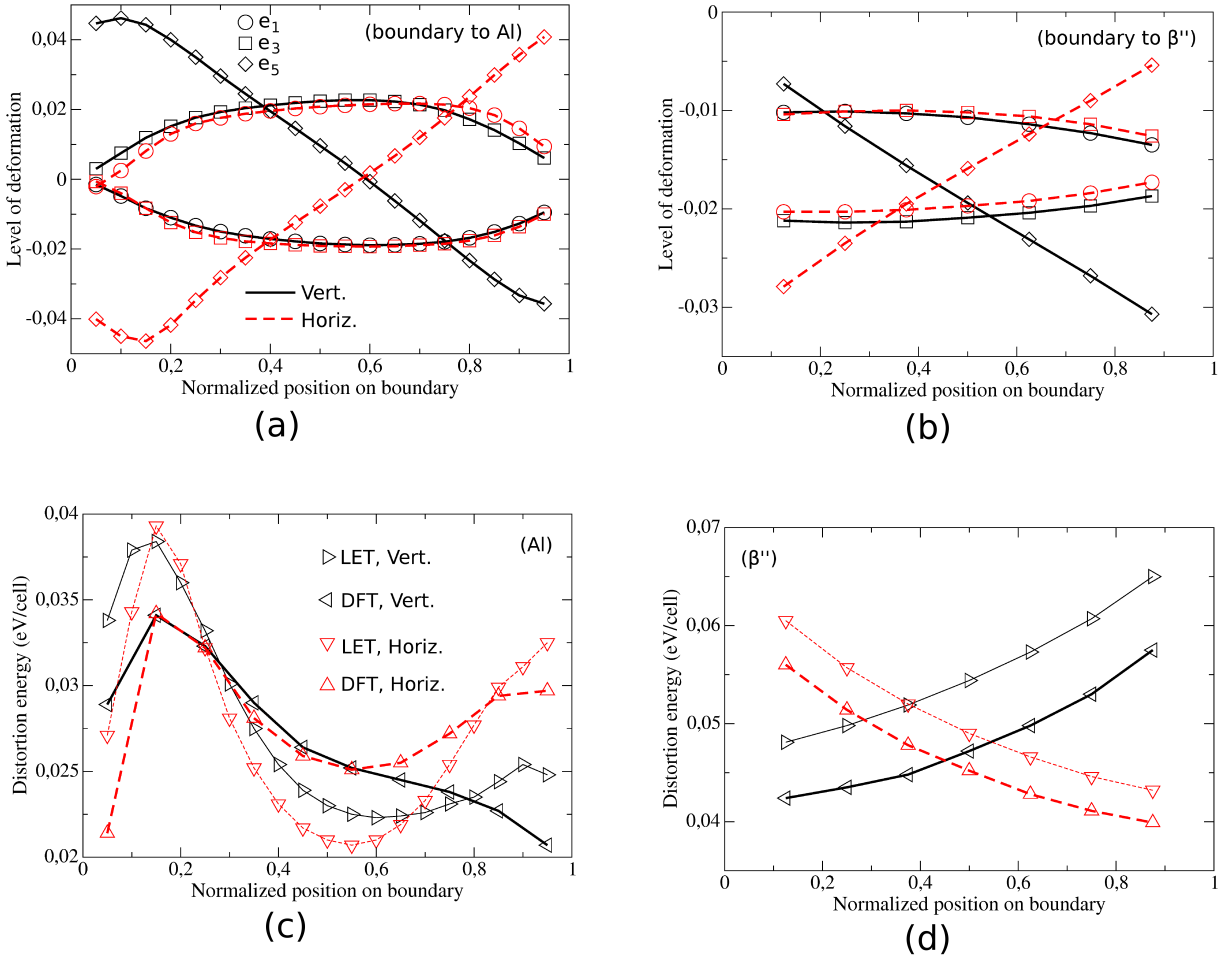

Figure 7. Calculated distortion parameters and energies at the DFT-LET boundaries shown schematically in figure 5. (*a*) Al distortions. (*b*) β" distortions. (*c*) Al energies. (*d*) β" energies. See text for details.

As shown in figures 7(*c*) and (*d*), a qualitative agreement of the DFT and LET distortion energies is encountered throughout. At the boundary to bulk Al, the LET energies are fluctuating around the DFT values with typical errors of ≈ 10%. Near the centre (corner), the LET values are lower (higher), with these two effects almost cancelling out upon averaging. At the boundary to bulk β", correlating with the differences between the structural data in figures 7(*a*) and (*b*), the cancellation of energy errors does not occur: the DFT energies are always lower (by ≈ 10%) than the LET counterparts. We note that while the errors made at the boundary to the precipitate are overall larger, corrections (if desired) should be easy to implement.

4.3. Interface region distortion parameters

From the FEM based results of section 4.1, the interface region distortion parameters, describing the evolution in local distortions along each interface, can be computed (see section 2.3). Figure 8 displays (*a*) the calculated adaptation parameters $\psi^{\mathbf{ab}}(i)$, $\psi^{\mathbf{cb}}(j)$, (*b*) the effective misfits $m_{\mathbf{a},\mathrm{eff}}(i)$, $m_{\mathbf{c},\mathrm{eff}}(j)$ and (*c*) the compression parameters $\kappa^{\mathbf{ab}}(i)$, $\kappa^{\mathbf{cb}}(j)$. Below, we discuss the values and variation of these quantities over the interface region, comparing with the results obtained for fully optimized supercells and the simple boundary condition employed in [11]. Technically, while the distortion parameters have been introduced in this work in the context of the FEM based structural boundary criterion, these quantities are well defined for all the above situations, through equations (6) – (9). In general, the variation in each interface region distortion parameter in figure 8 is noted to display close similarities when the **ab** and **cb** interface results are compared.

As shown in figure 8(*a*), the adaptation values for practically all interface region supercells exceed those obtained upon a full cell optimization – indicating that β" is adapting to a higher degree to the host lattice environment with the FEM based structural boundary condition introduced. This

criterion would seem expected: when a single supercell is fully relaxed, the precipitate and host lattice contributions are balanced, whereas in figure 4(*a*), the host lattice fully surrounds the precipitate, straining β" to a higher degree, as already shown in figure 7(*b*). Both adaptation parameters display a non-negligible, roughly linear variation along the interface, crossing the value 0.5 roughly at the point of zero shear strain on the supercell ($i = j = 0$). Comparing with figure 4(*a*), we find that the level of adaptation along both interfaces is increased when moving away from β_P, i.e., towards the 'sharp' precipitate corner. This may be viewed as an understandable precipitate relaxation mechanism, given that β" is less dominating locally at this point.

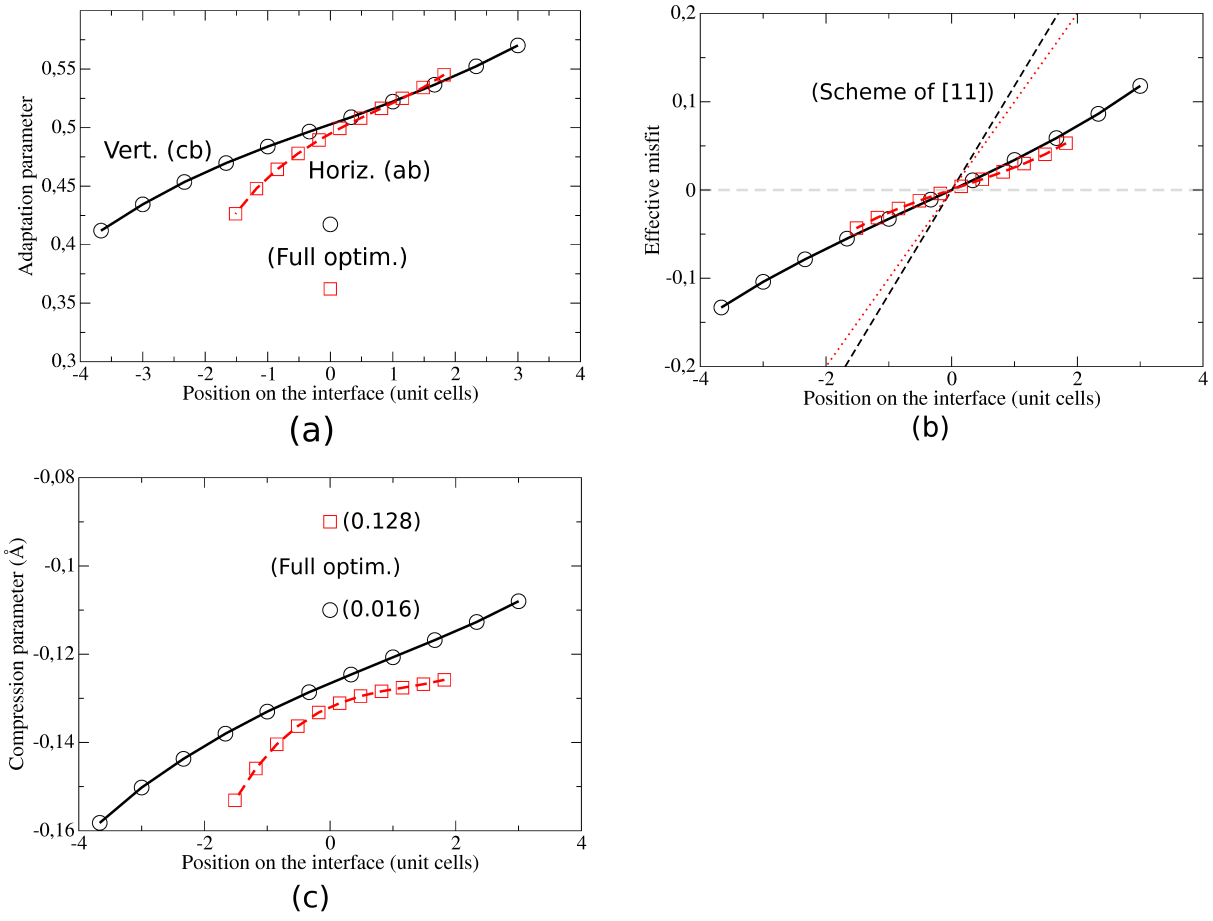

Figure 8. Calculated interface region distortion parameters (section 3.2.2) completely describing the interface region with the aid of equations (6) – (9). (*a*) Precipitate adaptation parameters $\psi^{ab}(i)$, $\psi^{cb}(j)$, describing the level to which β" conforms to the surrounding host lattice at the interface. (*b*)

Calculated effective misfits $m_{\mathbf{a},\mathrm{eff}}(i)$, $m_{\mathbf{c},\mathrm{eff}}(j)$ (obtained as half the slope of the curves shown), highlighting the evolution in the shear strain along the interface. (*c*) Interface region compression parameters $\kappa^{\mathbf{ab}}(i)$, $\kappa^{\mathbf{cb}}(j)$, highlighting the level of local compression normal to the interface. Results obtained within the earlier scheme of [11] are also shown.

For convenience, figure 8(*b*) shows the variation of $2im_{\mathbf{a},\mathrm{eff}}(i)$, $2jm_{\mathbf{c},\mathrm{eff}}(j)$ along the interface. This choice avoids a division with 2*i*, 2*j*, respectively, with these parameters both passing through zero. Both variations are closely linear (i.e., the effective misfits are almost constant), with $m_{\mathbf{a},\mathrm{eff}}(i) \approx 0.014$, $m_{\mathbf{c},\mathrm{eff}}(j) \approx 0.018$. These values are below $m_{\mathbf{a}}$ (= 0.05), $m_{\mathbf{c}}$ (= 0.06) by ≈ 76% and ≈ 70%, respectively, implying that the simple boundary condition of [11] is grossly exaggerating the strain evolution along each interface. Both the precipitate adaptation of figure 9(*a*) as well as the presence of significant host lattice strains at the interface region boundary (figure 7(*a*)) – compressing the precipitate and expanding the host, respectively – contribute to this significant difference.

The change in the compression parameter values when moving from a full supercell optimization to implementation of the FEM based structural boundary criterion of this work is profound. For both interfaces, the parameter *changes sign*, with a relative compression of ≈ 0.025 nm (0.015 nm) suggested in the vicinity of the **ab** (**cb**) interface. This result stresses the influence of the structural boundary condition to the interface energies, possibly to an even higher degree than the adaptation parameter modifications of figure 8(*a*). A variation in the parameters along the interface, resembling the result in figure 8(*a*) and with larger precipitate adaptation correlating with weaker compression, is noted.

To summarize, all interface region distortion parameters appear non-negligibly affected, in a manner qualitatively expected, when comparing the results of our multi-scale scheme with those of

[11]. The relative importance of these effects is unclear, with no studies involving introduction of each modification separately carried out in this work. However, in particular the compression parameter appears of interest, with the large difference reflecting the absence of constraints in [11] vs. the pure LET structural boundary criterion in the direction out of the interface in the multi-scale scheme. We shall return to this issue in Appendix C.

4.4. Interface energy determination

For clarity in the evaluation of the accuracy of the model scheme presented in this work, we divide the β"/Al system of figure 2 into three distinct volumes (see figure 9(*a*)): the precipitate (P), host lattice (H) and interface (PH) region. This division follows the basic ideas underlying the scheme, with comparatively large and weakly distorted regions subjected to a separate analysis. In particular, we would expect the main contributions to the β"/Al interface energy to be associated with the vicinity of the interface, the PH region.

Following the considerations in [11], the contributions to the zero temperature interface energy E_{Int} for a β"/Al slab geometry hosting a precipitate comprised by $N_{\mathbf{a}} \times N_{\mathbf{c}}$ unit cells along $\mathbf{a}_{\beta''}$, $\mathbf{c}_{\beta''}$, respectively, can be defined as follows (with the terms ordered according to distance to the precipitate centre):

$$E_{\mathrm{Int}} = \zeta_{\mathrm{P}} N_{\mathrm{P}} + \sum_i \{E_{\mathrm{PH}}(\mathbf{a}_i^{\mathbf{ab}}, \mathbf{b}_i^{\mathbf{ab}}, \mathbf{c}_i^{\mathbf{ab}}) - (N_{\mathrm{P}}^{\mathbf{ab}}/N^{\mathbf{ab}})E_{\mathrm{P}} - (N_{\mathrm{H}}^{\mathbf{ab}}/N^{\mathbf{ab}})E_{\mathrm{H}}\}$$

$$+ \sum_j \{E_{\mathrm{PH}}(\mathbf{a}_j^{\mathbf{cb}}, \mathbf{b}_j^{\mathbf{cb}}, \mathbf{c}_j^{\mathbf{cb}}) - (N_{\mathrm{P}}^{\mathbf{cb}}/N^{\mathbf{cb}})E_{\mathrm{P}} - (N_{\mathrm{H}}^{\mathbf{cb}}/N^{\mathbf{cb}})E_{\mathrm{H}}\} + \zeta_{\mathrm{H}} N_{\mathrm{H}};$$

$$i = \{-N_{\mathbf{a}}/2 + \delta_{\mathbf{a}}; \ldots; N_{\mathbf{a}}/2 + \delta_{\mathbf{a}}\}, j = \{-N_{\mathbf{c}}/2 + \delta_{\mathbf{c}}; \ldots; N_{\mathbf{c}}/2 + \delta_{\mathbf{c}}\}, \quad (20)$$

The first and last terms on the right hand side of equation (20) account for the strain energies in the P and H regions, respectively, and are derived by application of LET to the relevant subsystem (β",

Al), as implemented in the FEM based studies of section 3.1. As discussed earlier, interface electronic interactions are rendered negligible in these regions. The central terms (sums) in equation (20) denote the DFT calculated contributions to E_{Int} from the vicinity of the **ab** (sum over *i*) and the **cb** (sum over *j*) interfaces, i.e., the PH region energies. Here E_{PH} denotes the energy of an interface region supercell with e.g. the distorted cell *i* for the **ab** interface being defined through the basis vectors $\{\mathbf{a}_i^{\mathbf{ab}}, \mathbf{b}_i^{\mathbf{ab}}, \mathbf{c}_i^{\mathbf{ab}}\}$, obtained by aid of the DFT-LET boundary criterion as discussed in section 2.3.3. The set of basis vectors for all supercells considered has been included, along with the resulting supercell energies, in tables B1 and B2 of Appendix B. The labels *i* and *j* are both defined as zero at the point of vanishing shear strain at the respective interfaces (see figure 8(*b*)) – formally denoted $\delta_{\mathbf{a}}$, $\delta_{\mathbf{c}}$ in equation (20) – and running over the entire selected interface. The $N^{\mathbf{ab}}$ supercell atoms are shared between $N_{\mathrm{P}}^{\mathbf{ab}}$ precipitate atoms and $N_{\mathrm{H}}^{\mathbf{ab}}$ host atoms, i.e., $N^{\mathbf{ab}} = N_{\mathrm{P}}^{\mathbf{ab}} + N_{\mathrm{H}}^{\mathbf{ab}}$. By construction of the cells, see section 3.2, $N_{\mathrm{P}}^{\mathbf{ab}} = N_{\mathrm{H}}^{\mathbf{ab}}$ ($= N_{\mathrm{H}}^{\mathbf{cb}} = N_{\mathrm{P}}^{\mathbf{cb}}$) = 22. It follows (atom number conservation) that E_{P}, E_{H} – representing energies of *fully relaxed* subsystems – are obtained using the interface supercell geometry, but filling this region entirely with one subsystem. The sums in equation (20) consequently describe, within the modelling assumptions, the entire effect – structural and electronic – of the interacting subsystems, within the selected region (PH). The values of E_{P}, E_{H} have been included in table B3 of Appendix B. This appendix also briefly discusses how we converted E_{Int} to the units of kJ per mole, typically used in the literature.

Normally (see, e.g., [10, 25]), the interface energy contributions from the interface vicinity are separated into interfacial energy (σ) and strain energy (ζ_{PH}) contributions. While these separate quantities tend to be of interest on their own for understanding precipitate evolution, we have avoided this step in the present work. Firstly, a comparison of the interface energies E_{Int} as obtained using different model schemes should be sufficient for judging the overall precision of our scheme as compared to presently available alternatives. Secondly, the procedure in [10] provides no

information on how the separation into σ, ζ_{PH} should be performed when the supercell is strained in the direction normal to the interface. This latter issue is obviously of interest in its own right, but any discussions into the matter will be postponed until future work.

In section 4.5, we compare the findings obtained for the scheme of this work with the results of a 'conventional' model scheme roughly following the details outlined in [10]. Compared to equation (20), two key modifications are present in that earlier approach: firstly, the interfacial energy has been evaluated explicitly for fully optimized **ab** and **cb** interface region supercells, i.e., this quantity has been presumed constant along each interface. Secondly, the strain energies have been obtained everywhere directly from the FEM based results, i.e., within the framework of LET and avoiding the supercell construction described in section 2.3.3 [32]. We stress that the comparison of the two scheme approaches implies, in particular, that only the PH region energies are evaluated differently.

4.5. Calculated interface energy

Figure 9(*b*) shows the calculated contributions to the interface energy (also included in table 1) as obtained from the conventional analysis described in section 4.4. Roughly 70% of the total interface energy can be attributed to PH region contributions, with the interfacial energy – describing the electronic effects of the transition from precipitate to host lattice – exceeding the strain energy in this region by almost a factor three. The strain field tail into Al is noted to clearly exceed the strain energy within β". Recalling the conclusions of section 4.2 for the DFT-LET boundary criterion assessment, this result indicates that errors outside of the PH region in our model scheme should be of relatively little concern: in the P region, where the average difference between the DFT and LET distortion energies was clearly highest, the strain energy itself is by far the lowest.

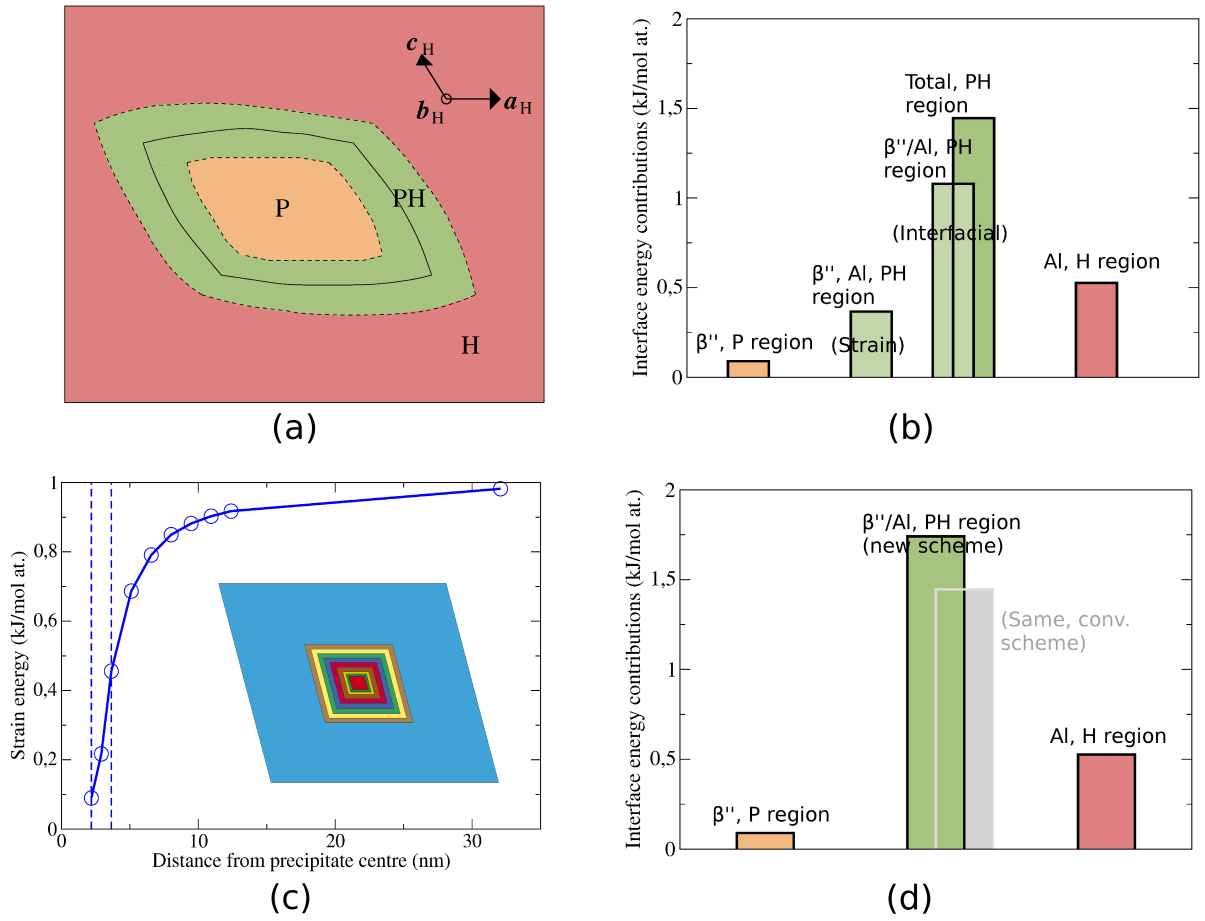

Figure 9. (*a*) Schematic presentation of the different regions P, PH and H where energy contributions are calculated separately in the FEM based analysis. DFT energies are computed only in region PH (the interface region). (*b*) Interface energy contributions as obtained within a conventional scheme: all strain energies have been computed within LET, while the interfacial energy is based on results for fully optimized interface region supercells. (*c*) Accumulated (LET) strain energy evolution with distance to the precipitate centre. The inset shows the regions from where each individual strain energy contribution was obtained, while the vertical lines through the curve highlight the interface region boundaries. (*d*) Interface energy contributions as obtained within the scheme of this work. The PH region energy is now calculated exclusively with DFT.

Figure 9(*c*) shows the evolution in the accumulated strain energy with distance from the precipitate centre, as calculated by summing energy contributions from the regions shown in the inset. This

presentation provides the additional important information of quantifying the behaviour of the strain field decay in the host lattice – making it possible to judge the errors made to the calculated interface energy when introducing a strain field cut-off distance r_C (see section 3.1). A strong support for a transition from a steep to a slow energy increase at 7 – 9 nm from the centre of β" is noted. This result combines well with the (independent) definition of r_C = 9.2 nm in section 3.1. We propose from this analysis that in order to ensure both acceptable accommodation of the strain field tail as well as weak errors due to precipitate interactions in a supercell based DFT description of the same system, a slab of size ≈ 18 × 18 nm², containing beyond 6000 atoms, would be needed. The full model system size slightly exceeds 3 × 3 β" cross-section dimensions. As we expect this requirement on the relative amount of host lattice and precipitate subsystems to be unaffected for a preserved β" (2D) aspect ratio, we can estimate the size of the smallest system where full DFT and multi-scale model results can be directly compared. Since our model scheme interpolates interface energies at the precipitate corners, a precipitate containing at the very least 3 × 3 primitive unit cells is required. This in turn suggests that a β"/Al model system containing ≈ 900 atoms is needed.

Figure 9(*d*) displays the interface energy contributions as obtained with our new scheme. As noted in section 4.4, changes are confined to the PH region. Here, the interface energy contribution, as compared with the conventional scheme, is increased by ≈ 20% (see table 1), resulting in a ≈ 14% increase in the full interface energy. Comparing with the conclusions in [11], this change is almost solely due to the modification of the structural boundary condition on the interface region supercells. In [11], two main conclusions were drawn from a similar comparison of interface energy determinations: *(i)* LET was incapable of predicting correctly the strain energy evolution along the interface. *(ii)* The resulting β" and Al subsystem strain energy errors were largely cancelling out, however, with no net energy change produced when comparing DFT and LET energies for the same set of supercells. In the present studies, the strain energy evolution along the interface is markedly

reduced (see figure 8(*b*)). However, a complete cancellation of subsystem LET errors must now seem absent, as judged from figure 9(*d*). We note that the potential influence of a significantly varying interfacial energy is neglected in this last argument for simplicity.

Table 1. Calculated contributions to the β"–$Mg_5Al_2Si_4$/Al interface energy for the system displayed schematically in figure 2(*a*), as obtained using three formalisms: a conventional model description (see text for details), the model scheme of this work, and the scheme of [11].

Contribution, region	Calculated value (kJ/mol at.)		
	(Conv. Scheme)	*(New scheme)*	*(Scheme of [11])*
Strain, P (β")	0.090	0.090	0
Strain, PH (β", Al)	0.366	-	-
Interfacial, PH (β"/Al)	1.079	-	-
Total, PH	1.445	1.741 (+20%)	2.044 (+41%)
Strain, H (Al)	0.526	0.526	0
Total	2.061	2.357 (+14%)	2.044 (–0.8%)

Table 1 also includes the interface energy as calculated with the scheme of [11]. Even though the strain field is entirely confined within the interface region in that earlier work, we would not necessarily expect a higher value of the calculated interface energy. As already indicated in section 4.3, the structural boundary condition used in [11] applies only along the interface, with full supercell relaxation in the direction out of the interface acting as strain relief, compared to the multi-scale scheme of the present work. A comparison of the full interface energies in table 1 shows that the interface energy is actually the *lowest* in the scheme of [11], and – presumably by

coincidence – very close to the conventional scheme value. Once again, this reflects the sensitivity of the quantity to model system structural modifications.

5. Potential model improvements

A number of assumptions, all of which merit further investigation, has been highlighted during the presentation of our proposed multi-scale model scheme. Firstly, the FEM based investigation of the full β"/Al system does not handle electronic interface effects, hence implicitly assuming zero interfacial energy. This is an obvious source of errors to the structural parameters in general (and the interface region boundary condition in particular), as the precipitate would show a desire to contract further if a more realistic value of σ were used. Conversely, in the DFT calculations, the structural influence of the electronic interface effects is neglected – once again indicating that the original FEM based parameters are taken at face value. Preliminary studies of Appendix C show that this assumption, while surprisingly accurate structurally, cannot be rigorously defended. Both of these issues highlight the simplicity of our approximation to the truly desired self-consistent coupling of the FEM and DFT based information on the system. However, considerable – and possibly even satisfactory – improvement may be obtained by implementing the two changes described above [33], whereas it is less certain that further fine tuning, with its added computational complexity, will yield 'comparable' levels of increased precision for the calculated energies. As already indicated in section 4.5, comparison with results of alternative schemes of undeniably higher accuracy would be of real interest as a means to obtain direct knowledge on the level of remaining errors in our scheme. Direct DFT studies appear rather prohibitive, whereas methods revolving around coarse graining techniques [34], [2] or a general attempted weak reduction in the basic theoretical framework accuracy [35], [36] may represent more feasible approaches.

The interface region boundary condition proposed for our scheme is explicitly *structural*, i.e., we assume that interface electronic effects are well contained within this region. While the work of [25] has provided some support for this hypothesis being defendable, a more rigorous testing of the choice of interface region supercell size may be needed. This issue is also of potential interest to the evaluation of the accuracy in the (necessary) interface energy interpolation procedure at the precipitate corners, see Appendix B, as such a procedure implicitly assumes short ranged interface electronic effects – and hence weak interaction between interfaces of different orientation. If electronic interface effects beyond the interface region need to be taken into account ultimately, the direct transition from a DFT to an LET region underlying our scheme is likely incapable of providing the desired accuracy [1, 37].

Other issues relate to precision in the more basic sense. The presumed most interesting factors are (*i*) the determination of the elastic constants underlying the whole scheme, (*ii*) the various assumptions connected with the 2D slab description and (*iii*) the level of precision when converting the FEM interface region into a patchwork of supercells each resting on PBCs. The first two topics should be addressed more or less by default during future developments of the scheme. As for the supercell construction errors, we compared the FEM structural input data for this scheme with the ultimate supercell dimensions for the various cells underlying equation (20). As expected, the main effect of the PBCs is an expansion (contraction) of the host lattice (precipitate) *along* the – highly misfit – interface. For the **cb** interface, values with a typical magnitude of $\approx 5 \times 10^{-3}$ nm, though higher for cells closer to the precipitate corners, are obtained at the largest distances to the interface. These numbers, which represent extremes of the PBC effects, should be compared to the bulk Al and β" misfit of 0.038 nm (see table A1). For the **ab** interface, similar conclusions can be obtained. When attempting to convert this structural information into estimated errors on the interface energy, additional information on the variation in the PBC effects from the actual interface location

(vanishing influence) to the interface region boundary (maximum influence) must seem required. Further, such energy considerations require knowledge on the range of the interface electronic effects, with a realistic procedure hence remaining rather uncertain at present. If these electronic effects are well contained in the supercell, the system energy will almost certainly be artificially *raised* due to the supercell construction, given that both subsystems experience enhanced distortion near the respective cell boundaries. Preliminary calculations based on this line of thought indicate energy corrections of a few percent of the PH region interface energy.

6. Summary and conclusion

In this work, we have outlined the details of an *ab initio* based hierarchical multi-scale model scheme for computation of the precipitate-host lattice interface energy E_{Int} for a fully coherent precipitate with compositionally sharp interfaces. We have used as our example case the main hardening phase β" of the Al–Mg–Si alloy system. Through preliminary LET modelling of a physically sized β"/Al system (2D slab chosen for simplicity throughout), we have provided two key ingredients of motivation for our scheme implementation. Near the interface, both subsystems are distorted, by way of their strong misfit in the precipitate cross-section plane, to levels where LET is no longer valid [11]. This calls for a DFT based description of a narrow (≈ nm width) band around the *whole* interface – the interface region. Further, even well into the host lattice, the strain field tail due to the subsystem interactions is still non-negligible, implying the preference for an LET based description over DFT investigations on a (necessarily) smaller system. Our scheme builds upon the theoretical framework described in [11] for *ab initio* based modelling of the full β"/Al interface. Compared to that work, we establish a coupling to the long range strain field by altering the interface region supercell structural boundary conditions based on an FEM simulation of the full β"/Al system. The key appealing factors of this coupling is its simplicity in terms of basic equations and computational effort, combined with expected improvement over [11]. At the

interface region boundary, subsystem (β", Al) energies as calculated with DFT and LET generally differ by 10% or less. Compared to a conventional model scheme [10], E_{Int} as calculated with our scheme has increased from 2.06 kJ per mole to 2.36 kJ per mole (≈ 14%) for the chosen β"–$Mg_5Al_2Si_4$/Al 2D slab geometry of investigation. This change is purely connected to the interface region, where the corresponding energy increase is 20%. With our model scheme being hierarchical, rather than truly hybrid, it remains to be clarified if these changes are primarily to be viewed as improvements (due to the use of DFT in the full interface region) or errors (due to the use of LET based interface region supercell dimensions). Future studies into this issue are encouraged.

Acknowledgements

This work has been financially supported by the Research Council of Norway via the MultiModAl project (project no. 205353). DFT simulations were performed through access to the NOTUR facilities.

Appendix A. Key input parameters to the β''/Al studies

Table A1 shows the calculated cell dimensions and basis vector angles for the β"–$Mg_5Al_2Si_4$ conventional cell, used here over the primitive cell counterparts (see section 3.2), in order to ease comparison with experimental values [16, 18]. The data shown were actually derived from a primitive cell study, by aid of the slight approximation $\gamma_{\beta''} = 74.5°$. The original values of this calculation are $a_{\beta''}^{\mathrm{Prim.}} = 0.7931$ nm; $b_{\beta''} = 0.4075$ nm; $c_{\beta''} = 0.6778$ nm; $\beta_{\beta''}^{\mathrm{Prim.}} = 105.4°$; $\gamma_{\beta''} = 74.9°$. Cell dimensions and angles for a corresponding Al supercell are shown in table A1 as well.

The resulting theoretical β"/Al misfit values in the precipitate cross-section clearly exceed the experimentally reported ones, with $m_{\mathbf{a}} = 5.0\%$ ($m_{\mathbf{c}} = 6.0\%$) as compared with the values 3.8% (5.3%) provided in section 2.1. Such a discrepancy is not unexpected, given that the precipitate

interactions with Al are ignored at this stage. When these interactions are included, compression of β" is obtained (see figure 7(*b*)), leading to a reduction in both theoretical misfit values. Given that only one β" configuration is investigated here, in a 2D slab set-up, quantitative discussions of the effects of this compression have been postponed until future work.

Table A1. Cell dimensions of fully relaxed bulk Al and β"–$Mg_5Al_2Si_4$ cells, as obtained with VASP. For the bulk Al system, deviations from perfect fcc Al with lattice parameter 0.4044 nm are negligible.

System	$\lvert\mathbf{a}_{\beta''}\rvert$ (nm)	$\lvert\mathbf{b}_{\beta''}\rvert$ (nm)	$\lvert\mathbf{c}_{\beta''}\rvert$ (nm)	β (°)
Al (β" supercell)	1.458	0.4041	0.6399	105.3
β"–$Mg_5Al_2Si_4$	1.532	0.4075	0.6778	105.9

The calculated elastic constants for bulk fcc Al and monoclinic β"–$Mg_5Al_2Si_4$ were obtained in previous work by Ehlers and Holmestad [11], see table 3 in that paper.

Appendix B. Key output parameters from the β''/Al studies

The calculated structural parameters used for the DFT based interface region investigations have been included in table B1 (**ab** or $(–320)_{Al}$ interface) and B2 (**cb** or $(130)_{Al}$ interface). The method for computing these parameters has been outlined in section 2.3.3. Conversion to interface energy contributions, using the two central terms in equation (20), requires, firstly, that the energies E_P, E_H of the fully relaxed bulk β"–$Mg_5Al_2Si_4$ precipitate and fcc Al host lattice systems be known. These values, as obtained from β" primitive unit cell and corresponding Al supercell studies, see Appendix A, are provided in table B3. Secondly, equation (20) requires that interface energy contributions be quantified also at the precipitate corners, outside the range of the data in tables B1

and B2. Here, an energy extrapolation was employed for each interface separately, i.e., the electronic interaction of the two interfaces was effectively neglected. We note that, given the nature of the FEM based structural boundary condition where interactions between the interfaces are not suppressed, this simple scheme may still contain a reasonable level of structural *interpolation* between the two interfaces, as desired. All energies introduced in this appendix have been specified in kJ/cell, where the term 'cell' denotes an interface region supercell, containing 44 atoms. For conversion of the output to units of kJ per mole, we weighted the individual energy contributions for the two sums in equation (20) appropriately, dividing the resulting energy with the number of atoms in the precipitate, $4 \times 8 \times 22 = 704$ (see figure 2(*b*)).

Table B1. Structural parameters and energies for the **ab** interface region supercells as obtained for the β"–$Mg_5Al_2Si_4$/Al system examined in this work. The cell dimension $\mathbf{b}^{ab}(i)$ has been kept fixed throughout as 0.4058 nm, see equation (5). In the calculations, β"/Al supercells based on the primitive β" cell were employed (see section 3.2), with the component along $\mathbf{b}_{\beta''}$ for $\mathbf{a}^{ab}(i)$ kept fixed as $\mathbf{b}^{ab}(i)/2$. In the table, this component was ignored, however, for easier comparison with the structural boundary considerations in the bulk text. The point $i = 0$, where the shear strain on the supercell is vanishing ($\beta^{ab}(i) = 105.3°$) is located at the normalized position ≈ 0.54, slightly away from the physical interface centre (normalized position 0.5). The parameter i denotes the movement in number of precipitate unit cells away from this centre, highlighting the above described asymmetry.

Norm. pos.	i (unit cells)	$\mathbf{a}^{ab}(i)$ (nm)	$\mathbf{c}^{ab}(i)$ (nm)	$\beta^{ab}(i)$ (°)	E_{PH} (10^{-20} kJ/cell)
0.0833	–1.82	0.7456	2.576	103.5	–2.488669
0.1667	–1.49	0.7460	2.580	104.0	–2.489178
0.2500	–1.15	0.7464	2.583	104.3	–2.489529

0.3333	–0.82	0.7467	2.586	104.6	–2.489778
0.4167	–0.49	0.7470	2.589	104.8	–2.489965
0.5000	–0.15	0.7473	2.592	105.1	–2.490080
0.5833	0.18	0.7477	2.594	105.3	–2.490142
0.6667	0.51	0.7481	2.596	105.6	–2.490149
0.7500	0.85	0.7486	2.599	105.9	–2.490094
0.8333	1.18	0.7492	2.601	106.2	–2.489944
0.9167	1.51	0.7500	2.604	106.5	–2.489657

Table B2. Structural parameters and energies for the **cb** interface region supercells as obtained for the β"–$Mg_5Al_2Si_4$/Al system examined in this work. See table B1 for basic details. The point $j = 0$ is located at the normalized position ≈ 0.54 on the interface.

Norm. pos.	j (unit cells)	$\mathbf{a}^{cb}(j)$ (nm)	$\mathbf{c}^{cb}(j)$ (nm)	$\beta^{cb}(j)$ (°)	E_{PH} (10^{-20} kJ/cell)
0.0833	–3.67	2.956	0.6615	106.8	–2.487727
0.1667	–3.00	2.954	0.6606	106.5	–2.487943
0.2500	–2.33	2.951	0.6599	106.1	–2.488066
0.3333	–1.67	2.949	0.6593	105.8	–2.488117
0.4167	–1.00	2.947	0.6588	105.6	–2.488108
0.5000	–0.33	2.945	0.6583	105.4	–2.488044
0.5833	0.33	2.943	0.6578	105.1	–2.487922
0.6667	1.00	2.940	0.6573	104.9	–2.487731
0.7500	1.67	2.938	0.6568	104.6	–2.487449
0.8333	2.33	2.935	0.6562	104.2	–2.487060
0.9167	3.00	2.932	0.6555	103.8	–2.486498

Table B3. Calculated system energies (β" primitive cell set-up, with resulting values scaled by four) for fully relaxed bulk β"–$Mg_5Al_2Si_4$ and fcc Al.

System	E_{PH} (10^{-20} kJ/cell)
Al	–2.602840
β"–$Mg_5Al_2Si_4$	–2.399847

Appendix C. Estimating the structural influence of interface electronic interactions

The hierarchical multi-scale model scheme described in the present work neglects any structural influence of the interface electronic interactions, with the FEM based formalism, providing the structural boundary condition for the interface region DFT studies, assuming negligible interfacial energy by default. We have avoided implementing any subsequent DFT correction to the interface region supercell widths in the bulk text. This choice was made partly for simplicity but also, such an approach would require direct modification of the FEM set-up as well for a rigorous DFT-LET structural boundary condition to still be operative. The present appendix will highlight an attempt to judge the importance of this issue, and hence quantify the necessity for improvements of our scheme in this context.

In section 2.3.2, we described how the cell dimension $\mathbf{c}^{ab}(i)$ should be obtained directly from the FEM output from the β"/Al system optimization. Confining ourselves here to the case of $i = 0$ for simplicity, we define a DFT correction to this quantity as follows: firstly, keeping the two cell basis vectors $\mathbf{a}^{ab}(0)$, $\mathbf{b}^{ab}(0)$ – defined through equations (10) and (5), respectively – fixed, we fully relax the interface region supercell along $\mathbf{c}_H$. This same conditional optimization is carried out as well using LET [38]. The difference in lengths $|\mathbf{c}^{ab}{}_{CORR}|$ between these optimized values of $|\mathbf{c}^{ab}(0)|$

constitutes the proposed DFT correction at the selected point on the interface. An equivalent approach applies to the cell dimension $\mathbf{a}^{\mathbf{cb}}(0)$.

The calculated values of $|\mathbf{c}^{\mathbf{ab}}_{\mathrm{CORR}}|$, $|\mathbf{a}^{\mathbf{cb}}_{\mathrm{CORR}}|$, are 0.020 nm and 0.009 nm, respectively – implying that, at the **cb** interface centre, e.g., the interface electronic effects would, roughly speaking, attempt to 'push out' the Al host lattice by 0.010 nm. Compared to the results of figure 8(*c*) on the compression parameter values with the presently used purely FEM based structural boundary condition, these modifications arguably appear non-negligible, with the associated energy changes indicating a lowering of the PH region interface energy contribution by several percent. At the same time, this modification should not be viewed entirely on its own, given that it must be counteracted by both a response from the surroundings and the use of a non-zero value of σ in the FEM based studies. The main conclusion of our preliminary consideration is that such direct incorporation of the interface electronic effects in both parts of the present model scheme is likely needed for a precision approaching a DFT simulation of the same system to be achieved.

References

[1] N. Bernstein, J. R. Kermode, and G. Csányi, Rep. Progr. Phys. **72**, 026501 (2009).

[2] P. Suryanarayana, V. Gavini, T. Blesgen, K. Bhattacharya and M. Ortiz, J. Mech. Phys. Solids **58**, 256 (2010).

[3] A. K. Nair, D. H. Warner, R. G. Hennig and W. A. Curtin, Scripta Mater. **63**, 1212 (2010).

[4] Y. Mishin, M. Asta and J. Li, Acta Mater. **58**, 1117 (2010).

[5] V. Vaithyanathan, C. Wolverton and L. Q. Chen, Phys. Rev. Lett. **88**, 125503 (2002).

[6] J. Allison, M. Li, C. Wolverton and X. Su, JOM **58**, 28 (2006).

[7] V. B. Shenoy, R. Miller, E. B. Tadmor, R. Phillips and M. Ortiz, Phys. Rev. Lett. **80**, 742 (1998).

[8] J. Q. Broughton, F. F. Abraham, N. Bernstein, E. Kaxiras, Phys. Rev. B **60**, 2391 (1999).

[9] J. Kermode, T. Albaret, D. Sherman, N. Bernstein, P. Gumbsch, M. C. Payne, G. Csányi and A. De Vita, Nature **455**, 1224 (2008).

[10] V. Vaithyanathan, C. Wolverton and L. Q. Chen, Acta Mater. **52**, 2973 (2004).

[11] F. J. H. Ehlers and R. Holmestad, Comp. Mater. Sci. **72**, 146 (2013).

[12] G. A. Edwards, K. Stiller, G. L. Dunlop, Appl. Surf. Sci. **76/77**, 219 (1994).

[13] C. D. Marioara, S. J. Andersen, J. Jansen and H. W. Zandbergen, Acta Mater. **51**, 789 (2003).

[14] G. A. Edwards, G. L. Dunlop and M. J. Couper, Conf. Proc., Georgia Institute of Technology, Atlanta, Georgia, 11 – 16 September 1994, appeared in ICAA4, Vol. 1, 1994, 620.

[15] H. W. Zandbergen, S. J. Andersen and J. Jansen, Science **277**, 1221 (1997).

[16] S. J. Andersen, H. W. Zandbergen, J. Jansen, C. Træholt, U. Tundal and O. Reiso, Acta Mater. **46**, 3283 (1998).

[17] We shall frequently use the notation **ab** and **cb** for the interfaces spanned by the precipitate vectors $\mathbf{a}_P$, $\mathbf{b}_P$ and $\mathbf{c}_P$, $\mathbf{b}_P$, respectively, as it connects more straightforwardly with the modelling considerations than conventional notation $(\bar{3}20)_{Al}$, $(130)_{Al}$.

[18] H. S. Hasting, A. G. Frøseth, S. J. Andersen, R. Vissers, J. C. Walmsley, C. D. Marioara, F. Danoix, W. Lefebvre, R. Holmestad, J. Appl. Phys. **106**, 123527 (2009).

[19] C. D. Marioara, S. J. Andersen, H. W. Zandbergen and R. Holmestad, Metal Mater. Trans. A **36A**, 691 (2005).

[20] J. D. Eshelby, Proc. Roy. Soc. A **24**, 376 (1957).

[21] C. Q. Ru, Acta Mech. **160**, 219 (2003).

[22] In practice, the accuracy in this coupling is always limited by the individual supercell periodic boundary conditions, even though cells for each point in the interface 'interior' (yielding smooth interface energy variations) are allowed. For further discussion, see section 5.

[23] C. Kittel, Introduction to Solid State Physics, 8th Ed., Wiley (2005), ISBN: 0-471-41526-X, p. 77.

[24] J.O. Hallquist, LS-DYNA Keyword User's Manual Version 971, California: Livermore Software Technology Corporation (2007).

[25] Y. Wang, Z.-K. Liu, L.-Q. Chen and C. Wolverton, Acta Mater. **55**, 5934 (2007).

[26] P. Hohenberg and W. Kohn, Phys. Rev. **136** B864 (1964).

[27] W. Kohn and L. J. Sham, Phys. Rev. **140** A1133 (1965).

[28] G. Kresse and J. Hafner, Phys. Rev. B **47** R558 (1993).

[29] G. Kresse and J. Furthmüller, Comput. Mater. Sci. **6**, 15 (1996).

[30] D. Vanderbilt, Phys. Rev. B **32**, 8412 (1985).

[31] J. P. Perdew, J. A. Chevary, S. H. Vosko, K. A. Jackson, M. R. Pederson, D. J. Singh, and C. Fiolhais, Phys. Rev. B **46**, 6671 (1992).

[32] Note that the procedure in [10] employed a single set of elastic constants for the system description in order to comply with the phase field modelling set-up. By contrast, we are using for our evaluation of this scheme the elastic constants of the two bulk subsystems β", Al, as described earlier.

[33] To implement a DFT based structural correction for each interface region supercell and retain a meaningful boundary condition to the surrounding parts of the system, one would have to introduce the same correction directly – in an ad hoc manner – in the FEM based studies, i.e., add a direct feedback (though not necessarily a full self-consistency loop) from the DFT calculations to FEM.

[34] G. Lu, E. Tadmor and E. Karixas, Phys. Rev. B **73**, 024108 (2006).

[35] D. R. Bowler and T. Miyazaki, Rep. Progr. Phys. **75**, 036503 (2012).

[36] I. Shin and E. A. Carter, Model. Simul. Mater. Sci. Eng. **20**, 015006 (2012).

[37] X. Zhang, G. Lu, and W. A. Curtin, Phys. Rev. B **87**, 054113 (2013).

[38] We stress that the result of this LET based optimization should not, in general, produce the length $|\mathbf{c}^{\mathbf{ab}}(0)|$ obtained from the FEM based optimization of the full β"/Al system. In the latter case, the **ab** interface is likely compressed along $\mathbf{c}_H$, whereas it is free to relax in the former optimization.